Review of Scientific Instruments

Catalyzed chemical polishing of SiO_2 glasses in pure water

Cite as: Rev. Sci. Instrum. **90**, 045115 (2019); https://doi.org/10.1063/1.5090320
Submitted: 26 January 2019 . Accepted: 19 March 2019 . Published Online: 15 April 2019

Daisetsu Toh, Pho Van Bui, Ai Isohashi, Naotaka Kidani, Satoshi Matsuyama, Yasuhisa Sano, Yoshitada Morikawa, and Kazuto Yamauchi

Review of Scientific Instruments ARTICLE scitation.org/journal/rsi

Catalyzed chemical polishing of SiO_2 glasses in pure water

Cite as: Rev. Sci. Instrum. 90, 045115 (2019); doi: 10.1063/1.5090320
Submitted: 26 January 2019 • Accepted: 19 March 2019 •
Published Online: 15 April 2019

Daisetsu Toh,[1] Pho Van Bui,[1,a)] Ai Isohashi,[1] Naotaka Kidani,[1] Satoshi Matsuyama,[1] Yasuhisa Sano,[1] Yoshitada Morikawa,[1,2] and Kazuto Yamauchi[1,2]

AFFILIATIONS

[1]Graduate School of Engineering, Department of Precision Science and Technology, Osaka University, 2-1 Yamada-oka, Suita, Osaka 565-0871, Japan
[2]Graduate School of Engineering, Research Center for Ultra-Precision Science and Technology, Osaka University, 2-1 Yamada-oka, Suita, Osaka 565-0871, Japan

[a)]buivanpho@up.prec.eng.osaka-u.ac.jp

ABSTRACT

A catalytically assisted etching system was developed for the ultra-precision fabrication of optical components, such as X-ray mirrors and extreme-ultraviolet mask blanks. This study demonstrates that an atomically smooth surface with a sub-Angstrom root-mean-square roughness could be achieved on a SiO_2 glass substrate using pure water and Pt as the etching solution and catalyst, respectively. Density functional theory calculations confirmed that the mechanistic pathway was involved in catalyzed hydrolysis. The significant roles of the catalyst were clarified to be the dissociation of water molecules and the stabilization of a meta-stable state, in which a hypervalent silicate state is induced, and the Si–O backbond is elongated and loosened. To confirm the role of the catalyst, the Pt metal was replaced by Au, and the observed drastic difference in the removal rate was attributed to the degree of stabilization of the metastable state.

I. INTRODUCTION

The demand for ultra-precision optical components is rapidly growing for scientific and industrial applications, especially in extreme ultraviolet (EUV) and X-ray regimes. Using ultra-precision optical systems with short wavelength light, major progress has been achieved in X-ray microscopy for the scientific imaging of cutting-edge materials and biological samples and in nanoscale lithography for next-generation semiconductor device fabrication.[1–4] However, the quality and the resolution of the optical devices and systems that fundamentally depend on the characteristics of the optical components remain critically important. Glass materials, such as pure and/or modified silica glasses, are still the main materials employed for optical components because of their attractive properties, such as low thermal deformation, cleanliness, machinability, and workability. Accordingly, significant advances have been made in the surface shaping and flattening of glass materials by ultra-precision finishing processes. However, several difficulties remain in producing the desired surfaces because of the high surface quality requirements. The polished surface must be atomically smooth with a root mean square (rms) roughness at the level of several tens of picometers to maximize reflectivity and reduce unwanted scattering.[5–9] Any subsurface damage or irregularity that remains on the optical surface can decrease the performance and accelerate a system failure. The chemical mechanical polishing (CMP) method is generally used to finish these surfaces.[10–12] In the CMP method, a pad is employed to scrub the sample surface with a slurry containing SiO_2 and CeO_2 particles as abrasives.[13–16] The removal is predominantly based on the mechanical effects of the abrasives with a synergetic effect of the chemicals added in the slurry. Although these chemicals in the slurry can reduce mechanical damage and irregularities, such as scratches, bumps, and pits can be inadvertently induced on the surface by unwanted mechanical attacks.[17,18] Thus, an abrasive-free polishing method employing catalyzed chemical etching, known as catalyst-referred etching (CARE), has been developed.[19–21] While the apparatus for CARE is nearly the same as that of CMP, the technique mainly differs in the addition of a catalytic function on the pad surface by the deposition of a thin catalyst film. The etching solution itself should not react with the work surface without the aid of the catalyst. During processing, the

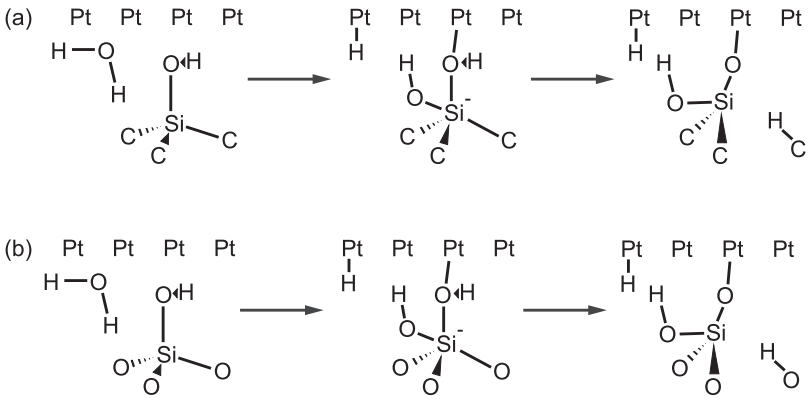

FIG. 1. (a) CARE reaction pathway for the etching of SiC using Pt catalyst and water, and (b) proposed reaction pathway for SiO_2. In these schemes, the backbonds of SiC or SiO_2 are elongated.

topmost area on the work surface more frequently contacts with the catalyst, and chemical etching proceeds at the contacted areas. Accordingly, the topmost parts of the work surface are preferentially etched, as is generally required in a polishing method. Consequently, CARE could ensure a highly ordered surface both geometrically and crystallographically.

Recently, a 4H-SiC wafer was successfully planarized using this technique with Pt and pure water as the catalyst and the etching solution, respectively.[21] An atomically smooth surface with a straight step-terrace structure having a height of one bilayer of 4H-SiC was obtained.[21] The CARE removal mechanism has been clarified as the indirect dissociative adsorption of a water molecule to break a Si–C bond.[22] In other words, this is a hydrolysis reaction. The reaction pathway is shown in Fig. 1(a). A water molecule dissociates with the assistance of Pt, and OH^- adsorbs on the step-edge Si to form a hypervalent silicate (5-fold coordination of Si) as a meta-stable state (MS). The total energy of the MS is reduced by forming Pt–O–Si bonds at the Pt–SiC interface. In the hypervalent silicate state, the Si–C backbond is elongated and loosened, promoting the transfer of a proton to the backbond to break the bond. The roles of the Pt catalyst were elucidated to be assistance with water dissociation and stabilization of the hypervalent silicate state through interface bonding by forming Pt–O–Si chains (22).

The CARE process is expected to be more applicable to SiO_2 materials; the Si–O bond has a relatively higher ionicity, which is an attractive property that can facilitate the hydrolysis reaction [Fig. 1(b)]. The aim of this work, therefore, is to demonstrate the potential of SiO_2 planarization using CARE in water and understand the characteristics of the process. In addition, the removal mechanism is discussed using density functional theory (DFT) calculations.

II. EXPERIMENTAL METHODS

A 2-in. quartz glass wafer was employed as a typical amorphous SiO_2 material. A 2-in. α-quartz ($10\bar{1}1$) on-axis (r-face on-axis cut) was also employed as a typical crystalline material to investigate the removal characteristics of CARE. A schematic of the apparatus used in this study is shown in Fig. 2. A Pt thin film was deposited as the catalyst on an elastic pad, which had narrow grooves on its surface. The sample was placed into a holder and pressed onto the pad with a pressure of 40 kPa by an airbag placed behind the work. The work and the pad were immersed in pure water and rotated independently at slightly different speeds near 10 rpm. Although the pad surface was relatively rough (such as 1 μm rms), a geometrically highly ordered surface could be obtained owing to an averaging effect by the random motion between the pad and the work, which is also a general idea for realizing smoothing in conventional CMP methods. To control the electrochemical potential of the Pt catalyst, which has been reported to be a significant parameter in

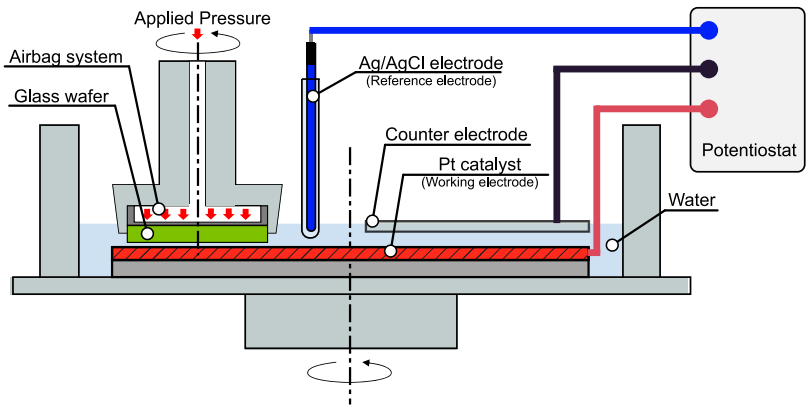

FIG. 2. Schematic of the apparatus similar to a general polishing machine. A wafer and a polishing pad are immersed in pure water. The work is set in the holder and faces toward the pad with a pressure of 40 kPa by an airbag placed behind the work. The three-electrode system is equipped with an Ag/AgCl electrode employed as the reference electrode.

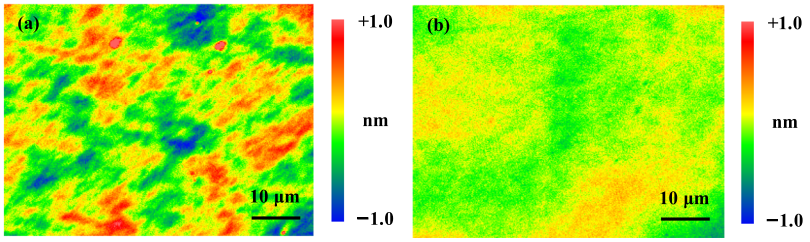

FIG. 3. Optical profiler images of the (a) pre-processed surface (P–V: 17.472 nm, rms: 0.612 nm, Ra: 0.496) and (b) CARE-processed surface of silica glass (P–V: 1.196 nm, rms: 0.127 nm; Ra: 0.099 nm).

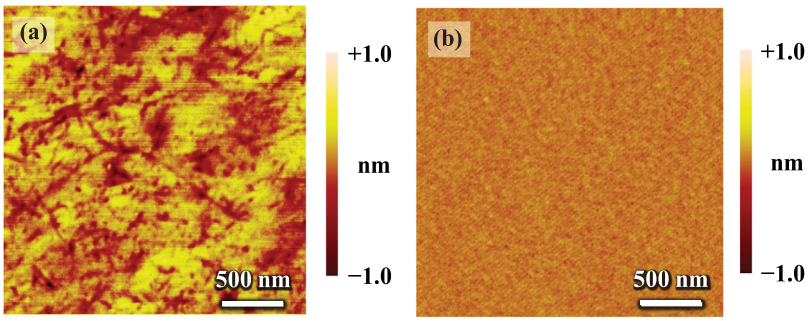

FIG. 4. AFM images of the (a) pre-processed (P–V: 2.056 nm, rms: 0.173 nm) and (b) CARE-processed (P–V: 1.169 nm, rms: 0.046 nm) silica glass surfaces.

material removal rates (MRRs),[21] we used a three-electrode system with a potentiostat. The potentials are discussed using the potential difference vs the standard hydrogen electrode (SHE).

Under open-circuit conditions, the self-potential of the Pt catalyst was approximately 0.25 V. The MRRs were investigated under potentials ranging from −0.6 to 1.2 V to avoid the generation of gaseous products (hydrogen and oxygen) on the Pt surface. The surface morphologies before and after CARE were observed with a phase-shift interference microscope (ZYGO NewView 200CHR) and an atomic force microscope (AFM; Digital Instruments Dimension 3100). The MRRs were estimated from the weight loss of the work.

III. RESULTS AND DISCUSSION

A. Surface planarization

Figures 3(a) and 3(b) show the surface profiles of the pre- and CARE-processed surfaces of silica glass, respectively. The roughness in peak-to-valley (P–V) and rms is markedly improved.

Figures 4(a) and 4(b), respectively, show AFM images of a silica glass wafer before and after CARE processing. The roughness is drastically reduced from 0.173 to 0.046 nm rms, indicating that the surface is atomically smooth.

Figures 5(a) and 5(b), respectively, show AFM images of α-quartz surfaces before and after CARE processing. In contrast to the surface showing a high degree of roughness and multiple scratches before CARE processing, the CARE-processed surface shows a clear step-and-terrace structure which is highly ordered. Figure 5(c) represents a two-dimensional profile along the dashed line in Fig. 5(b). The profile indicates a step height of approximately 0.34 nm, which corresponds to the height of one bilayer of the quartz crystal.

The step-and-terrace structure obtained after CARE processing on the quartz wafer suggests that etching occurs only at the step edges, meaning that the removal process is based on the step-flow etching phenomenon. The MRRs of the crystalline quartz and the silica glass are 6.6 and 200 nm/h, respectively. The MRR of the glass material is much higher than that of the crystalline material. On the

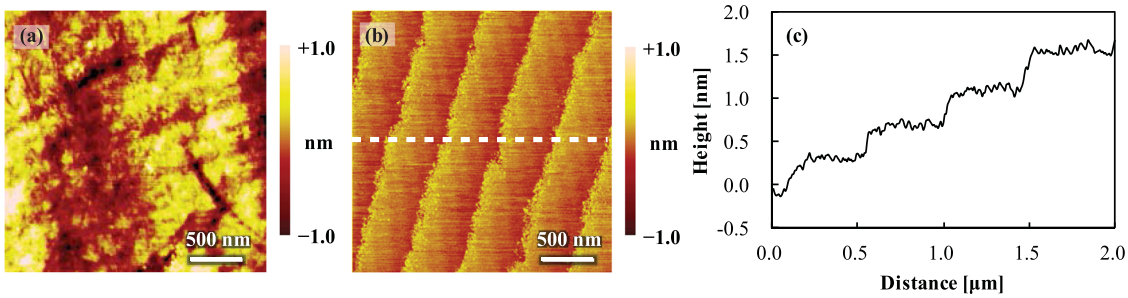

FIG. 5. AFM images of the (a) pre-processed surface of the r-face quartz (PV: 3.431 nm, rms: 0.145 nm) and (b) CARE-processed surface of the r-face quartz (P–V: 1.405 nm, rms: 0.131 nm). The line profile of the height along the white dashed line in (b) is shown in (c). The step height is approximately 0.34 nm, which corresponds to the height of one bilayer of the quartz crystal structure.

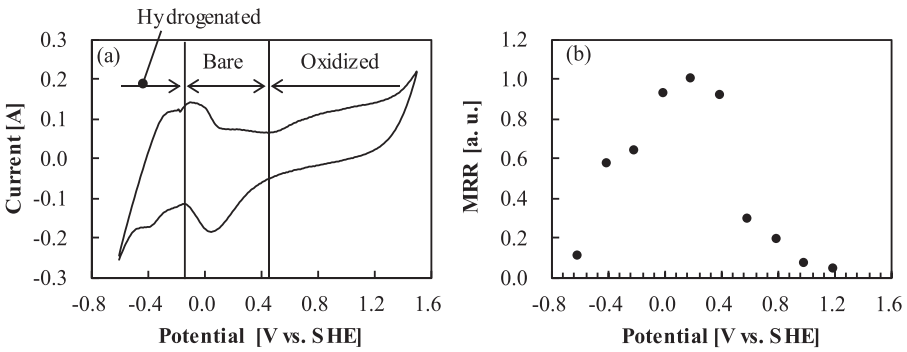

FIG. 6. (a) Cyclic voltammogram of Pt measured at a scan rate of 0.5 V/s. The characteristics of chemisorption on Pt are illustrated. (b) Dependence of the relative material removal rates (MRRs) upon the electrochemical potential of Pt; the MRR obtained at the self-potential was determined to be 1.0 (b).

crystal surface, etching proceeds at only the step edges, which are present on the surface at a lower density when the surface orientation is in the low-order index.[23] In contrast, in amorphous materials, the surface consists of atomic-height undulations which could provide sites at which etching can proceed. Therefore, the MRR of the silica glass is higher than that of the crystalline quartz.

B. Dependence on the electrochemical potential of the catalyst surface

The MRR of SiC depended on the electrochemical potential of the Pt catalyst.[21] The surface potential of the catalyst was observed via cyclic voltammetry using the three-electrode potentiostat system shown in Fig. 2; the obtained cyclic voltammogram is shown in Fig. 6(a). The Pt catalyst surface is, respectively, hydrogenated, oxidized, and bare when the potential is below −0.2 V, above 0.4 V, and between these two potentials. The dependence of the MRR on the electrochemical potential of the Pt catalyst is shown in Fig. 6(b). The highest MRR is obtained at about 0.2 V, and etching hardly proceeds at potentials below −0.6 V or above 1.0 V. These results suggest that the MRR is higher when the Pt surface is bare and decreases with the increase of hydrogen or oxygen adsorption. These adsorbates could hinder hydrolysis reactions at the SiO_2–Pt interface, leading to the low experimentally observed MRR. These results exhibit nearly the same trends as those from the CARE of SiC. A bare Pt atom on the surface can more effectively play the critical roles of dissociating a water molecule and stabilizing the hypervalent silicate state. From a practical point of view, since the 0.25 V open-circuit potential of the Pt catalyst is nearly appropriate, it would not be necessary to equip a potential control system on the CARE instrument. To more deeply confirm this modeling, we changed the catalyst from Pt to Au, which is the noblest metal and has much lower catalytic ability than Pt.[24] The MRR in the case of the Au catalyst is drastically reduced to nearly zero, as shown in Fig. 7. This result indicates the strong dependence on the catalyst metal and can be explained in terms of the two significant roles of the catalyst, which confirm the validity of our model.

C. First-principles analysis

To confirm the hydrolysis mechanism and the role of the catalyst in the CARE of silica glass and quartz, we performed first-principles calculations to estimate the activation barriers of the relevant reaction pathways and understand the different characteristics of the Pt and Au catalysts. The calculation methods are explained in the Appendix. The calculation models were prepared following the reaction pathway proposed in Fig. 1(b). Atomic positions at each step of the pathway were converged until the total force acting on each atom was less than 10^{-3} E_h/a_0, where E_h = 27.211 eV and a_0 = 0.529 Å.

The converged initial states (IS), MS, and final states (FS) with the Pt and Au catalysts are shown in Figs. 8(a) and 8(b), respectively. The activation barriers in the cases of the Pt and Au catalysts were calculated as 0.8 and 2.1 eV (Fig. 9). For the Pt catalyst, the activation barrier of 0.8 eV is low enough such that the reaction proceeds under room temperature. In contrast, the activation barrier using the Au catalyst is 2.1 eV, which means that etching hardly proceeds at room temperature, in agreement with the nearly zero MRR observed experimentally. We can also understand the detailed differences between the Pt and Au catalysts from Fig. 9. The energy of the MS is significantly stabilized in the case of the Pt catalyst, leading to the low activation barrier, and consequently, to the high removal rate. This is due to atomic interactions through the Pt–O–Si bonds at the interface. The highest nobleness of Au results in weak interactions at the interface and lowers the stability of the MS. This can be directly determined from the shape of the energy diagram in Fig. 9. Qualitatively, the diagrams of the Pt and Au cases are the same; only the position of the MS is shifted to be higher energy in the case of the Au catalyst. Here, we can provisionally conclude that the removal rate becomes higher when the MS is stabilized. However, from another perspective, when the bonding strength of M–O–Si (M = Pt or Au) is excessively strong, the reaction product covers the catalyst surface and hinders the CARE reaction. The catalyst

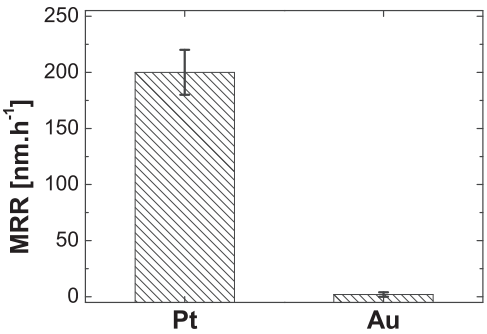

FIG. 7. MRRs of silica glass processing via CARE using Pt and Au catalysts.

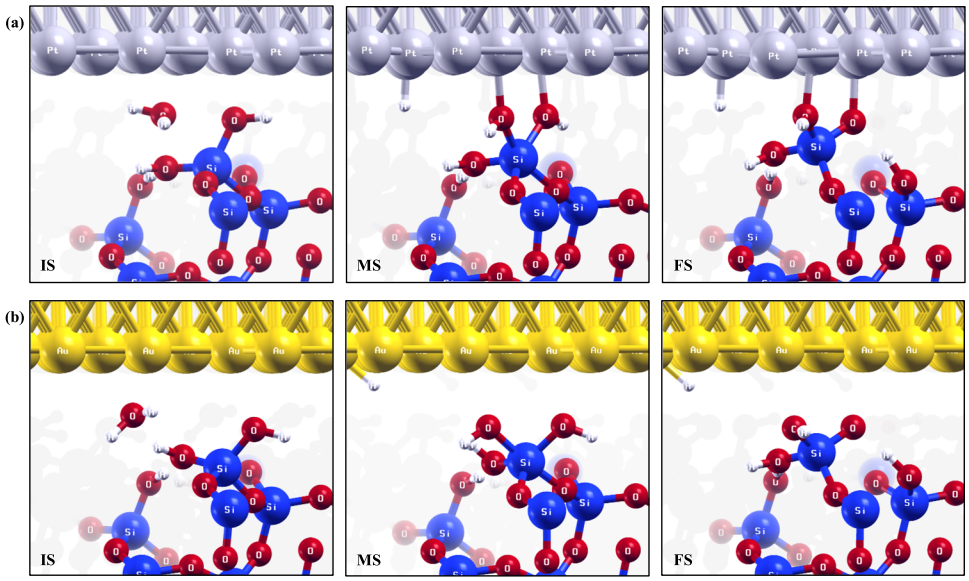

FIG. 8. Atomic geometries of the initial state (IS), meta-stable state (MS), and final state (FS) for the (a) Pt and (b) Au catalysts. Similar pathways and positions of the catalyst layer were used.

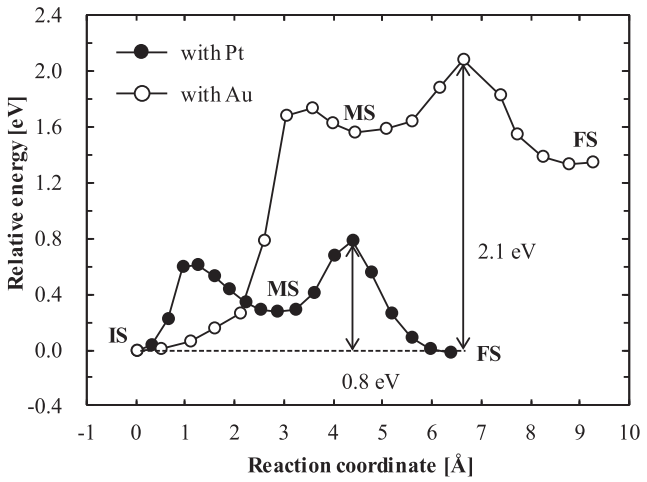

FIG. 9. Reaction energy profiles for indirect hydrolysis onto a Si–O bond for the models using Pt (●) and Au (○) catalysts.

surface must be repeatedly refreshed to ensure continuity of the CARE reaction. In future studies, the bonding strength of M–O–Si can be optimized by investigating appropriate metal catalysts.

IV. SUMMARY

This study demonstrated the application of CARE planarization to SiO_2 glass substrates using a Pt catalyst in pure water. The CARE-processed surfaces were atomically smoothed. For crystalline SiO_2 (quartz), an ultimately smoothed surface having a step-and-terrace structure with one-bilayer-high steps was produced.

The catalytic reactivity of the Pt catalyst was examined by changing its electrochemical potential; the MRR exhibited a strong dependence on the potential. The results indicated that the bare surface of the Pt catalyst was the most appropriate for the CARE reaction, having shown the same trend as in the case of SiC etching. The MRR was significantly decreased when the catalyst surface was covered by adsorbates of H and OH. Practically, at the open circuit potential of 0.25 V, the MRR becomes nearly maximum; thus, intentional control of the Pt potential is unnecessary.

From the first-principles calculation, the significant roles of the catalyst are the dissociation of water molecules and stabilization of the MS, in which a hypervalent silicate state is induced at the target Si atom and the backbond elongates, loosens, and is easily etched away. The stabilization originated from the Pt–O–Si bonding at the interface between the surfaces of the work and the catalyst. The MRR becomes nearly zero when the catalyst is changed from Pt to Au. In the latter case, the MS state is not sufficiently stabilized, which leads to a higher reaction barrier. However, excessive stabilization due to strong bonding at M–O–Si might lead to coverage of the catalyst surface by the reaction products, which would hinder the CARE reaction. Optimization of the degree of stabilization can be achieved by selecting the appropriate catalyst.

With the elucidated mechanism, the CARE of SiO_2 glass materials becomes not only a practical ultra-precision polishing method for next-generation optical devices but also an environmentally friendly and sustainable polishing technology because of its abrasive- and chemical-free character.

ACKNOWLEDGMENTS

This work was partially supported by JSPS KAKENHI (Grant Nos. JP16H06358, JP16J06391, JP14J01623, and JP18J20252). Numerical calculations were performed in the computer centers at Osaka University, the Institute for Solid State Physics, the University of Tokyo, and Tohoku University.

APPENDIX: CALCULATION METHOD AND MODEL

The Simulation Tool for Atom Technology (STATE) program package was employed.[25,26] The calculations were based on

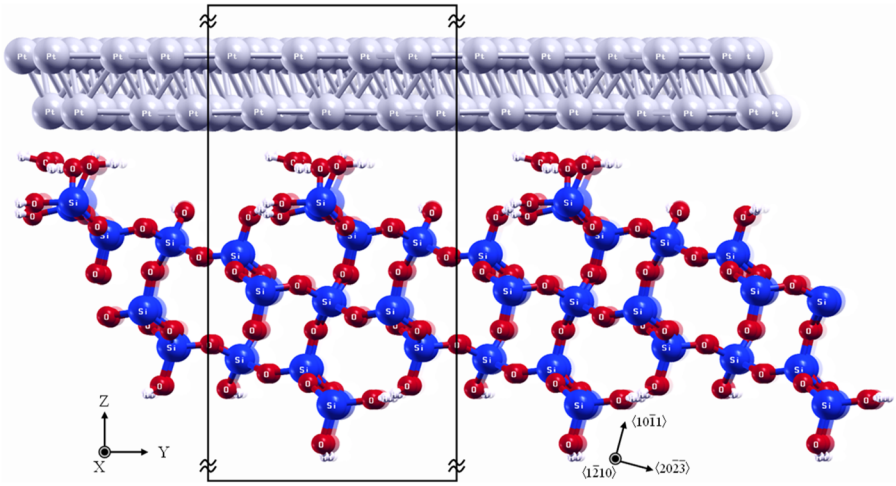

FIG. 10. Side view of the α-quartz (10$\bar{1}$1) model with a step-terrace structure. The box indicates a unit cell in the calculation.

DFT within the generalized gradient approximation proposed by Perdew.[27] The electron–ion charge interactions were described by ultra-soft pseudopotentials.[28] A 3 × 2 × 1 uniform *k*-point mesh was used in the entire surface Brillouin zone. The climbing-image nudged-elastic band method (CI-NEB) was adopted to calculate the reaction pathways.[29,30] The wavefunction and the charge density were expanded by a plane-wave basis set with cutoff energies of 25 and 225 Ry, respectively. Optimization was iteratively performed until the residual forces acting on all the atoms at the saddle point were reduced to below 10^{-3} E_h/a_0, where E_h = 27.211 eV and a_0 = 0.529 Å. All the simulations were conducted at zero temperature.

A slab model containing a stepped α-quartz (10$\bar{1}$1) surface, which is similar to the surface structure observed after CARE, and Pt (111) layers with a bare surface, are shown in Fig. 10. The successive slab was separated by a vacuum region with a thickness of approximately 20 Å in a direction normal to the Pt (111) surface. The fundamental removal mechanisms of quartz and silica glass were anticipated to be similar; hence, we employed the α-quartz (10$\bar{1}$1) model. The Si atoms at the topmost surface and the bottom layer were terminated by OH because the quartz surface is known to form silanol groups. During the simulations, the adsorbates, the two topmost bilayers of quartz along with the terminated atoms, and the bottom layer of Pt were allowed to fully relax, while the remaining atoms were kept fixed in position to maintain the substrate and Pt (111) structure. In the case of Au, the simulations were conducted with the same slab model containing the α-quartz (10$\bar{1}$1) surface shown in Fig. 10 and an Au (111) layer with a bare surface. To avoid the high compressive stress at the interface, the relative distance between the Pt and the quartz surfaces was validated by the total force exerted on the Pt and Au layers along the z-direction, in which the total force was from 1 to 2.5 nN at each step in the proposed reaction pathways. This force was low enough and comparable to the mean value of the force between the probing and a sample in an AFM operated in non-contact mode.[31,32]

REFERENCES

[1] D. A. Shapiro, Y.-S. Yu, T. Tyliszczak, J. Cabana, R. Celestre, W. Chao, K. Kaznatcheev, A. L. D. Kilcoyne, F. Maia, S. Marchesini, Y. S. Meng, T. Warwick, L. L. Yang, and H. A. Padmore, Nat. Photonics **8**, 765 (2014).
[2] C. Wagner and N. Harned, Nat. Photonics **4**, 24 (2010).
[3] A. Sakdinawat and D. Attwood, Nat. Photonics **4**, 840 (2010).
[4] F. Calegari, D. Ayuso, A. Trabattoni, and L. Belshaw, Science **346**, 336 (2014).
[5] W. M. Tong, J. S. Taylor, S. D. Hector, and M. K. Shell, Proc. SPIE **3873**, 421 (1999).
[6] The Micropatterning Global Technical Committee, SEMI P37-0613—Specification for Extreme Ultraviolet Lithography Substrates and Blanks, Microlithography, 2013.
[7] C. W. Gwyn, R. Stulen, D. Sweeney, and D. Attwood, J. Vac. Sci. Technol., B: Microelectron. Nanometer Struct. **16**, 3142 (1998).
[8] R. J. Noll, Opt. Eng. **19**, 192249 (1980).
[9] D. E. Savage, J. Kleiner, N. Schimke, Y.-H. Phang, T. Jankowski, J. Jacobs, R. Kariotis, and M. G. Lagally, J. Appl. Phys. **69**, 1411 (1991).
[10] L. M. Cook, J. Non-Cryst. Solids **120**, 152 (1990).
[11] R. Komanduri, D. A. Lucca, and Y. Tani, CIRP Ann. **46/2**, 545 (1997).
[12] P. B. Zantye, A. Kumar, and A. K. Sikder, Mater. Sci. Eng.: R: Rep. **45**, 89 (2004).
[13] S.-H. Lee, Z. Lu, S. V. Babu, and E. Matijević, J. Mater. Res. **17**, 2744 (2002).
[14] M. Sivanandini, S. S. Dham, and B. S. Pabla, Int. J. Adv. Res. Technol. **1**, 1 (2012).
[15] S. Kishii, K. Nakamura, K. Hanawa, S. Watanabe, Y. Arimoto, S. Kurokawa, and T. K. Doi, Jpn. J. Appl. Phys., Part 2 **51**, 04DB07 (2012).
[16] A. Beaucamp, Y. Namba, and P. Charlton, Appl. Opt. **53**, 3075 (2014).
[17] R. V. Randive, A. Ma, P. A. Kearney, D. Krick, I. Reiss, P. B. Mirkarimi, and E. Spiller, Proc. SPIE **5**, 023003 (2006).
[18] M. Upadhyaya, A. Basavalingappa, H. Herbol, and G. Denbeaux, J. Vac. Sci. Technol., B: Microelectron. Nanometer Struct. **33**, 021602 (2015).
[19] H. Hara, Y. Sano, H. Murata, K. Arima, A. Kubota, K. Yagi, J. Murata, and K. Yamauchi, J. Electron. Mater. **35**, L11 (2006).
[20] Y. Sano, K. Arima, and K. Yamauchi, ECS J. Solid State Sci. Technol. **2**, N3028 (2013).
[21] A. Isohashi, P. V. Bui, D. Toh, S. Matsuyama, Y. Sano, K. Inagaki, Y. Morikawa, and K. Yamauchi, Appl. Phys. Lett. **110**, 201601 (2017).
[22] P. V. Bui, D. Toh, A. Isohashi, S. Matsuyama, K. Inagaki, Y. Sano, K. Yamauchi, and Y. Morikawa, Jpn. J. Appl. Phys., Part 2 **57**, 055703 (2018).
[23] T. Okamoto, Y. Sano, K. Tachibana, K. Arima, A. N. Hattori, K. Yagi, J. Murata, S. Sadakuni, and K. Yamauchi, J. Nanosci. Nanotechnol. **11**, 2928 (2011).

[24]B. Hamber and J. K. Norkov, Nature **376**, 238 (1995).
[25]T. Hayashi, Y. Morikawa, and H. Nozoye, J. Chem. Phys. **114**, 7615 (2001).
[26]Y. Morikawa, Phys. Rev. B **63**, 033405 (2001).
[27]J. P. Predew, K. Burke, and M. Ernzerhof, Phys. Rev. Lett. **77**, 3865 (1996).
[28]D. Vanderbilt, Phys. Rev. B **41**, 7892 (1990).
[29]G. Mills, H. Jónsson, and G. K. Schenter, Surf. Sci. **324**, 305 (1994).
[30]G. Henkelman, B. P. Uberuaga, and H. Jónsson, J. Chem. Phys. **113**, 9901 (2000).
[31]A. Campbellova, M. Ondracek, P. Pou, R. Perez, P. Klapetek, and P. Jelinek, Nanotechnology **22**, 295710 (2011).
[32]Y. Sugimoto, P. Pou, M. Abe, P. Jelinek, R. Perez, S. Morita, and O. Custance, Nature **446**, 64 (2007).